

Preparation and Characterization of Simulated Crud

E. H. Lee*, S. H. Kim, K. M. Kim, J. W. Na, B. S. Choi, and W. Y. Maeng
Nuclear Materials Research Division, Korea Atomic Energy Research Institute,
1045 Daedeok Street, Yuseong, Daejeon 305-353, Republic of Korea
*ehlee@kaeri.re.kr

1. Introduction

Corrosion products, in the primary-side systems of pressurized-water reactors (PWRs), can be deposited on a fuel's surfaces. Accumulation of these corrosion products, mainly composed of nickel ferrite, nickel oxide, and iron oxides, leads to an axially un-symmetric heat flux depression, which decreases the heat efficiency of a fuel. In order to solve this problem, a formation mechanism of nickel-iron mixed oxides and then a possible mechanism for a deposition of corrosion products should be elucidated. The present work deals with the synthesis of nickel-iron oxide powders and the measurements of characteristics of the as-prepared powders.

2. Methods and Results

2.1 Materials and Test Procedures

The used chemicals were nickel (II) nitrate hexahydrate ($\text{Ni}(\text{NO}_3)_2 \cdot 6\text{H}_2\text{O}$), iron (III) nitrate nonahydrate ($\text{Fe}(\text{NO}_3)_3 \cdot 9\text{H}_2\text{O}$), lithium hydroxide monohydrate ($\text{LiOH} \cdot \text{H}_2\text{O}$), boric acid (H_3BO_3), and lithium metaborate (LiBO_2). Solutions with molar ratio of Ni:Fe=1:2 and 1:1 were prepared by dissolving $\text{Ni}(\text{NO}_3)_2 \cdot 6\text{H}_2\text{O}$ and $\text{Fe}(\text{NO}_3)_3 \cdot 9\text{H}_2\text{O}$ in de-ionized water. After 1 h stirring, a co-precipitator (2 M LiOH) was added to the solution and aged for 3 h with stirring at room temperature. The resultant precipitate was washed with de-ionized water and then filtered using a vacuum pump, which was repeated three times. Four samples with different conditions were prepared in this study. Samples with a molar ratio of Ni:Fe = 1:2 denoted as S1 and with a molar ratio of Ni:Fe = 1:1 denoted as S2, S3, S4, respectively. S1 and S2 samples were washed with de-ionized water but not S3 because of investigating a pH effect. To examine the effect of H_3BO_3 , S4 was washed with 1800 ppm (as B) H_3BO_3 solution after final washing and filtering. The obtained precipitates were dried in a vacuum oven at 70°C for 24 h and then ground to use as starting materials for this work. TGA/DSC and XRD were measured to identify phases of the samples.

2.2 Thermal Behaviors of Precursors

Fig. 1 and Fig. 2 present TG/DSC curves of the as-prepared precursors that were obtained by the co-

precipitation between $\text{Ni}(\text{NO}_3)_2 \cdot 6\text{H}_2\text{O}$ and $\text{Fe}(\text{NO}_3)_3 \cdot 9\text{H}_2\text{O}$ in water containing LiOH and H_3BO_3 and then by drying in the vacuum oven. After TGA analyses the resultant powders were examined by using the XRD, which is shown in Fig. 3. The first weight losses, as shown in Fig. 1, are due to the water in iron (III) - nickel (II) mixed hydroxides with or without containing boron, no significant differences could be observed below 150°C . As the temperature increases mass losses also increased continuously, however, no further mass changes were observed above 450°C . This may indicate the transformation and decomposition reactions have terminated in the co-precipitated materials. The final weight losses of S1, S2, S3, and S4 co-precipitates were about 22 %, 25 %, 30 %, and 22 %, respectively. The reason for the highest weight loss of the S3 is that the S3 co-precipitate was not washed with deionized water. As a result, it has more decomposing nitrate (NO_3^-) ions than others (S1, S2, S4). Fig. 2 presents DSC thermograms of the as-prepared precursors. For S1 with a molar ratio of Ni:Fe = 1:2, two endothermic reactions occurred. The DSC curve indicating a broad band at about 131.0°C contributes to a loss of water in the S1 and another broad band at about 390.2°C corresponds to transformation of amorphous iron (III) - nickel (II) mixed hydroxides into nickel ferrite (NiFe_2O_4). These results were consistent with the XRD patterns shown in Fig. 3. In this work, no hematite (Fe_2O_3) phase appeared, however other workers observed Fe_2O_3 phase [1, 2]. During TGA measuring ($10^\circ\text{C}/\text{min}$, from 0°C to 1000°C), it seems that there is no enough time to form Fe_2O_3 phase. For S2 and S3 with a molar ratio of Ni:Fe = 1:1, three endothermic reactions occurred at temperature range from 120°C to 420°C . Peak intensities of nickel ferrite (NiFe_2O_4) are not higher than that of S1. First endothermic reaction resulted from the loss of water and dehydration in the S2 and S3. At the second endothermic reactions, iron (III) - nickel (II) mixed hydroxides of S2 and S3 transformed into nickel oxide (NiO) due to Ni-rich chemical compositions, confirmed by the XRD patterns (Fig. 3). The last endothermic reactions correspond to the transformation of iron (III) - nickel (II) mixed hydroxides into NiFe_2O_4 , which is also evidenced by the XRD data as shown in Fig. 3. However, for S3 without washing deionized water all the endothermic peaks were shifted to lower temperatures and peak intensities are also lower than that of S2. For S4 with a molar ratio of Ni:Fe = 1:1 and

washing with 1800 ppm H_3BO_3 solution, the DSC curve indicating two endothermic bands at about $144.4^\circ C$ corresponds to a loss of water and another very broad endothermic band at about $387.7^\circ C$ contributes to the formation of $NiFe_2O_4$, bonaccordite ($Ni_2Fe(BO_3)O_2$), and vonsenite ($Fe_2Fe(BO_3)O_2$).

3. Conclusions

Nickel-Iron and Nickel-Iron-Boron oxides were synthesized and characterized. Bonaccordite which is suspected to be a root cause of AOA was examined by using a XRD.

REFERENCES

- [1] J. W. Yeon, K. S. Choi, Y. Jung, S. Rengaraj, Y. K. Ha, and W. H. Kim, Study on Nickel Ferrite Formation by Using a Simple Method to Simulate Heat Transfer Surfaces, Solid State Phenomena, Vol. 124-126, pp. 1565-1568, 2007.
[2] J. A. Sawicki, Evidence of Ni_2FeBO_5 and $m-ZrO_2$ precipitates in fuel rod deposits in AOA-affected high boiling duty PWR core, J. Nuclear Materials, Vol.374, pp.248-269, 2008.

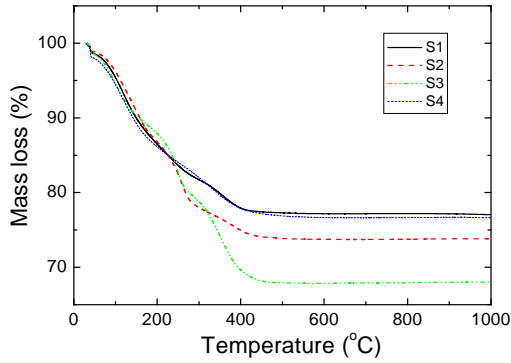


Fig. 1. TGA curves of the as-prepared precursors.

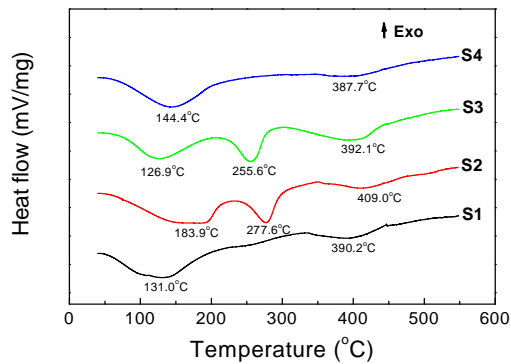


Fig. 2. DSC curves of the as-prepared precursors

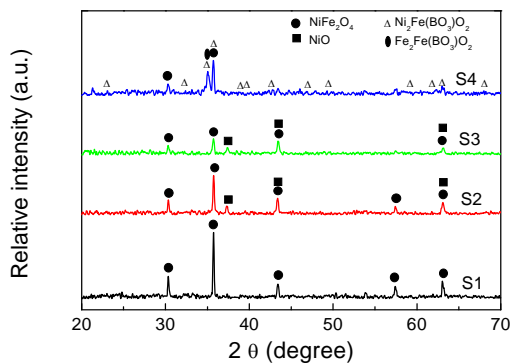


Fig. 3. XRD results of the samples after analyses of TGA.